Hypothalamic extended synaptotagmin-3 contributes to the development of dietary obesity and related metabolic disorders

Yi Zhang[a,b,c,1], Yunliang Guan[a,b,c,1], Susu Pan[a,b,c,1], Lihong Yan[d,e,1], Ping Wang[a,b,c], Zhuo Chen[a,b,c], Qing Shen[a,b,c], Faming Zhao[a,b,c], Xin Zhang[d,e], Juan Li[a,b,c], Juxue Li[d,e,2], Dongsheng Cai[f,2], and Guo Zhang[a,b,c,2]

[a]Department of Toxicology, Key Laboratory of Environmental Health, Ministry of Education, School of Public Health, Tongji Medical College, Huazhong University of Science and Technology, Wuhan, Hubei 430030, China; [b]Institute for Brain Research, Huazhong University of Science and Technology, Wuhan, Hubei 430030, China; [c]Collaborative Innovation Center for Brain Science, Huazhong University of Science and Technology, Wuhan, Hubei 430030, China; [d]State Key Laboratory of Reproductive Medicine, Nanjing Medical University, Nanjing, Jiangsu 211166, China; [e]Key Laboratory of Human Functional Genomics of Jiangsu Province, Nanjing Medical University, Nanjing, Jiangsu 211166, China; and [f]Department of Molecular Pharmacology, Albert Einstein College of Medicine, Bronx, NY 10461

Edited by Gerald I. Shulman, Yale University, New Haven, CT, and approved July 1, 2020 (received for review March 12, 2020)

The C_2 domain containing protein extended synaptotagmin (E-Syt) plays important roles in both lipid homeostasis and the intracellular signaling; however, its role in physiology remains largely unknown. Here, we show that hypothalamic E-Syt3 plays a critical role in diet-induced obesity (DIO). E-Syt3 is characteristically expressed in the hypothalamic nuclei. Whole-body or proopiomelanocortin (POMC) neuron-specific ablation of *E-Syt3* ameliorated DIO and related comorbidities, including glucose intolerance and dyslipidemia. Conversely, overexpression of E-Syt3 in the arcuate nucleus moderately promoted food intake and impaired energy expenditure, leading to increased weight gain. Mechanistically, *E-Syt3* ablation led to increased processing of POMC to α-melanocyte-stimulating hormone (α-MSH), increased activities of protein kinase C and activator protein-1, and enhanced expression of prohormone convertases. These findings reveal a previously unappreciated role for hypothalamic E-Syt3 in DIO and related metabolic disorders.

extended synaptotagmin 3 | hypothalamus | POMC neuron | obesity | glucose intolerance

The C_2 domain is a conserved sequence motif and the second most common Ca^{2+} binding module in the proteome (1). Proteins containing this domain are mainly involved in membrane trafficking and signal transduction, with synaptotagmin (Syt) and protein kinase C (PKC) as the prime examples. To date, studies have identified four families of membrane trafficking protein, including Syt, extended synaptotagmin (E-Syt), ferlin, and multiple C_2 domain and transmembrane region protein (MCTP) (2). The E-Syt protein family comprises E-Syt1, E-Syt2, and E-Syt3 in the mammalian cells, which functions as PtdIns(4,5)P_2 and Ca^{2+}-dependent (E-Syt1) or -independent (E-Syt2 and E-Syt3) endoplasmic reticulum (ER)-plasma membrane (PM) tether (3, 4). Recent studies showed that E-Syts play a key role in the lipid homeostasis of PM (5–7). E-Syt2 was found to mediate the endocytosis of fibroblast growth factor receptor (8), whereas loss of all of the ER-PM tether proteins, including orthologs of E-Syt, resulted in the separation of ER from PM and the activation of the unfolded protein response in yeast (9). E-Syts are expressed in the brain and peripheral tissues, such as lung, spleen, and testis (10). Attempts to unveil the physiological function of E-Syts by using *E-Syt2* and *E-Syt3* double, or *E-Syt1, E-Syt2*, and *E-Syt3* triple-knockout (*KO*) mice did not reveal any appreciable roles in animals' development, viability, reproduction, and brain morphology (10–12). Also, histological assessment did not identify any abnormality in the lung, spleen, testis, muscle, and brain in the *E-Syt2* and *E-Syt3* double-*KO* mice (10). Thus, it remains unclear regarding the roles of E-Syt proteins in physiology and/or pathology.

The hypothalamus is the center controlling animal's energy homeostasis. Neurons located in the arcuate (Arc), ventromedial (VMH), dorsomedial (DMH), and paraventricular (PVH) nuclei, as well as the lateral hypothalamic area (LH), are involved in the regulation of energy balance. In Arc nucleus, among the many transcriptionally distinct cell types (13), POMC and Agouti-related peptide (AgRP)-expressing neurons are the best-characterized ones in energy metabolism. Deficiency of POMC or melanocortin 4 receptor (MC4R), the receptor for POMC-derived neuropeptide, α-melanocyte-stimulating hormone (α-MSH), resulted in hyperphagia and obesity in both human subjects and animal models (14–18). Moreover, recent studies showed that there was impaired processing of POMC to α-MSH in the DIO mice (19, 20), suggesting rectification of this process may have the potential to mitigate obesity. Previously, we have shown that Syt-4 negatively regulates the exocytosis of oxytocin in the PVH, while this regulation was found impaired in the condition of DIO (21). With interest, we report in the current study that E-Syt3

Significance

The epidemic of obesity has reached an alarming level worldwide. Understanding the etiology of obesity is important for identifying a new approach of prevention or treatment. Accumulating evidence demonstrates that the central nervous system plays a critical role in animal's energy homeostasis. Here, we show that extended synaptotagmin (E-Syt3) is expressed in the hypothalamus and contributes to diet-induced obesity development. Whole-body or proopiomelanocortin neuron-specific deletion of *E-Syt3* significantly protects mice against DIO and related metabolic disorders. Mechanistically, we show that inhibition of *E-Syt3* can lead to increased hypothalamic content of α-melanocyte-stimulating hormone. Thus, our current work suggests that E-Syt3 might be a relevant target for treating obesity.

Author contributions: Y.Z., Y.G., S.P., L.Y., P.W., Z.C., Q.S., Juxue Li, D.C., and G.Z. designed research; Y.Z., Y.G., S.P., L.Y., P.W., Z.C., Q.S., F.Z., X.Z., and Juan Li performed research; Y.Z., Y.G., S.P., L.Y., P.W., Z.C., Q.S., F.Z., X.Z., Juan Li, Juxue Li, and G.Z. analyzed data; D.C. and G.Z. wrote the paper; and G.Z. conceived the study.

The authors declare no competing interest.

This article is a PNAS Direct Submission.

[1]Y.Z., Y.G., S.P., and L.Y. contributed equally to this work.

[2]To whom correspondence may be addressed. Email: lijuxue@njmu.edu.cn, dongsheng.cai@einstein.yu.edu, or gzhang@hust.edu.cn.

This article contains supporting information online at https://www.pnas.org/lookup/suppl/doi:10.1073/pnas.2004392117/-/DCSupplemental.

First published August 3, 2020.

works mainly in a different hypothalamic region and in a distinct manner to affect energy balance and obesity development.

Results

E-Syt3 Is Characteristically Expressed in Mouse Hypothalamus. To characterize the expression of E-Syt3, we did whole mount X-Gal staining on adult *E-Syt3* heterozygous mice, in which the expression of β-galactosidase (β-Gal) is under the control of transcriptional regulation elements of *E-Syt3* (10, 12). Interestingly, X-Gal product was mostly concentrated along the midline of hypothalamus, suggesting expression of *E-Syt3* in this region (Fig. 1 *A* and *B*). X-Gal staining of tissue sections did not reveal any obvious signal in the cerebral cortex, thalamus, epididymal white adipose tissue (eWAT), brown adipose tissue, skeletal muscle, and cardiac muscle (Fig. 1 *C* and *D* and *SI Appendix*, Fig. S1 *A–D*). There was weak staining in the hippocampus, liver, and pituitary (Fig. 1*E* and *SI Appendix*, Fig. S1 *E* and *F*). However, X-Gal staining yielded a strong signal in the hypothalamus, particularly in the Arc, VMH, and DMH nuclei (Fig. 1*F*), suggesting expression of *E-Syt3* in these regions. There were a few X-Gal–positive cells in the LH (Fig. 1*G*), but none were observed in the PVH (Fig. 1*H*). We then examined the cell type in which E-Syt3 is expressed. To this end, we performed combined X-Gal and immunohistochemical staining for NeuN and GFAP, which are markers for neurons and astrocytes, respectively. The results demonstrated that E-Syt3 is predominantly expressed in neurons, but barely detectable in astrocytes (Fig. 1*I*), suggesting that it may have a role in hypothalamic neuronal regulation of physiology.

Whole-Body Ablation of *E-Syt3* Ameliorates DIO and Related Comorbidities. The hypothalamus-enriched expression of E-Syt3 might suggest that it plays a role in affecting energy balance. To study this question, we generated whole-body *E-Syt3 KO* (10, 12) (*SI Appendix*, Fig. S2*A*) and littermate wildtype (*WT*) mice. Western blot and RT-PCR analyses of hypothalamus showed that both the protein and the mRNA of *E-Syt3* were absent in the *KO* mice (Fig. 2*A* and *SI Appendix*, Fig. S2*B*). At the age of 6 wk, chow-fed male E-Syt3 *WT* and *KO* mice did not differ in body weight (*SI Appendix*, Fig. S2*C*). These mice were then fed a high-fat diet (HFD), or maintained on the regular chow. Under chow condition, body-weight gain of *E-Syt3 KO* mice was comparable to that of *WT* controls (Fig. 2*B*). However, *E-Syt3 KO* mice gained significantly less body weight than *WT* animals when fed an HFD (Fig. 2*B*), indicating that E-Syt3 is involved in developing DIO. There was significantly less fat mass in HFD-fed *E-Syt3 KO* mice compared with *WT* controls (Fig. 2*C*), while the lean mass remained comparable (Fig. 2*D*). Consistently, adipocytes of eWAT were smaller in size (Fig. 2*E* and *SI Appendix*, Fig. S2*D*), and plasma leptin level was reduced in HFD-fed *E-Syt3 KO* compared with *WT* mice (Fig. 2*F*).

Glucose intolerance was improved in HFD-fed *E-Syt3 KO* mice compared with *WT* controls (Fig. 2 *G* and *H*). Consistently, the size of pancreatic islet was smaller (*SI Appendix*, Fig. S2*E*), and the plasma insulin level was lower in *E-Syt3 KO* mice than *WT* controls (Fig. 2*I*), further demonstrating the better handling of blood glucose. Under HFD condition, liver and plasma triglycerides (TG), as well as plasma total cholesterol (TC) levels were significantly reduced in *E-Syt3 KO* mice compared with those of *WT* controls (Fig. 2 *J–L*). Notably, these parameters did not differ between *E-Syt3 WT and KO* mice under chow condition (Fig. 2 *G–L* and *SI Appendix*, Fig. S2 *F–H*). Collectively, these data demonstrate that ablation of *E-Syt3* improves glucose intolerance and the dysregulation of lipid metabolism in DIO mice.

The antiobesity phenotype in *E-Syt3 KO* mice suggests that energy balance in these animals has been negatively shifted. Thus, we assessed the food intake, interscapular temperature, and energy expenditure of *E-Syt3 WT* and *KO* mice. We observed that *E-Syt3 KO* mice consumed considerably less HFD (Fig. 2*M*). These *KO* mice also demonstrated higher interscapular temperature than *WT* controls (Fig. 2 *N* and *O*). Both parameters remained comparable when the mice were fed the chow diet (Fig. 2*M* and *SI Appendix*, Fig. S2 *I* and *J*). Moreover, HFD-fed *E-Syt3 KO* mice consumed more oxygen and produced more heat than *WT* littermates (Fig. 2 *P* and *Q*). Taken together, these data suggest that *E-Syt3* deficiency could ameliorate DIO and related metabolic disorders.

Overexpression of E-Syt3 in Arc Neurons Leads to Obesity and Obesity-Related Syndrome. We then performed a gain-of-function study to address how overexpressing E-Syt3 in the Arc could affect metabolic balance. We constructed a neuron-specific, E-Syt3–expressing lentiviral plasmid (hereafter E-Syt3-Lenti), in which the transcription of mouse E-Syt3 cDNA is under the control of *Synapsin I* promoter (22). The enhanced green fluorescent protein (EGFP)-expressing vector was used as an experimental control (Ctrl-Lenti). We produced and delivered these lentiviruses into the Arc nucleus of *E-Syt3 WT* mice (Fig. 3*A*), which were maintained on the regular chow diet. Western blot analysis showed that E-Syt3 protein level was elevated in the Arc of mice infected with E-Syt3-Lenti viruses (Fig. 3*B*). Overexpression of E-Syt3 did not impact neuronal survival (*SI Appendix*, Fig. S3 *A* and *B*); however, these mice gained more body weight than the controls (Fig. 3*C*), which was mainly due to the increasing of fat mass (Fig. 3 *D–F* and *SI Appendix*, Fig. S3 *C* and *D*). Moreover, overexpression of E-Syt3 in Arc neurons led to hypertriglyceridemia, hypercholesterolemia, and glucose intolerance (Fig. 3 *G–J*). The appetite was modestly increased, and the interscapular temperature was decreased in these mice (Fig. 3 *K–M*). A further assessment showed that these mice consumed less oxygen, and produced less carbon dioxide as well as heat (Fig. 3 *N–P*). Taken together, these data indicate that overexpression of E-Syt3 in Arc neurons could positively shift energy balance.

POMC Neuron-Specific Deletion of *E-Syt3* Protects Mice against DIO. It is well established that POMC neurons in the Arc nucleus play a critical role in energy balance. An initial assessment using immunofluorescent staining for E-Syt3 and α-MSH showed that E-Syt3 is expressed in POMC neurons (*SI Appendix*, Fig. S4*C*). We then crossed the *E-Syt3 KO* mice with *Flp* mice (23) to generate the $E\text{-}Syt3^{Loxp/Loxp}$ mice (*SI Appendix*, Fig. S4*A*). The $E\text{-}Syt3^{Loxp/Loxp}$ mice were further mated with *POMC-Cre* mice (24) to generate the *POMC-Cre*, $E\text{-}Syt3^{Loxp/Loxp}$ mice in which *E-Syt3* is selectively deleted in POMC neurons (*SI Appendix*, Fig. S4 *A* and *B*), as well as the littermate *POMC-Cre* and $E\text{-}Syt3^{Loxp/Loxp}$ mice. Immunofluorescent staining data showed that E-Syt3 protein was efficiently eliminated from the POMC neurons (*SI Appendix*, Fig. S4 *C–F*). As expected, the percentage of E-Syt3–expressing neurons among all neurons in the Arc was significantly reduced in the *POMC-Cre,* $E\text{-}Syt3^{Loxp/Loxp}$ mice (65.4 ± 3.0%, 64.9 ± 3.7%, and 50.1 ± 3.8% for the *POMC-Cre*, $E\text{-}Syt3^{Loxp/Loxp}$, and *POMC-Cre,* $E\text{-}Syt3^{Loxp/Loxp}$ mice. $P < 0.05$, *POMC-Cre* or $E\text{-}Syt3^{Loxp/Loxp}$ versus *POMC-Cre,* $E\text{-}Syt3^{Loxp/Loxp}$, one-way ANOVA with Bonferroni's posthoc test, $n = 4–5$ mice per group). Given that Cre driven by *POMC* transcriptional control elements is also expressed in the adrenocorticotropic hormone (ACTH)-expressing cells in pituitary, we examined the morphology of pituitary and adrenal gland. The results demonstrated that tissue morphology and the expression of ACTH in pituitary were comparable among the three genotypes (*SI*

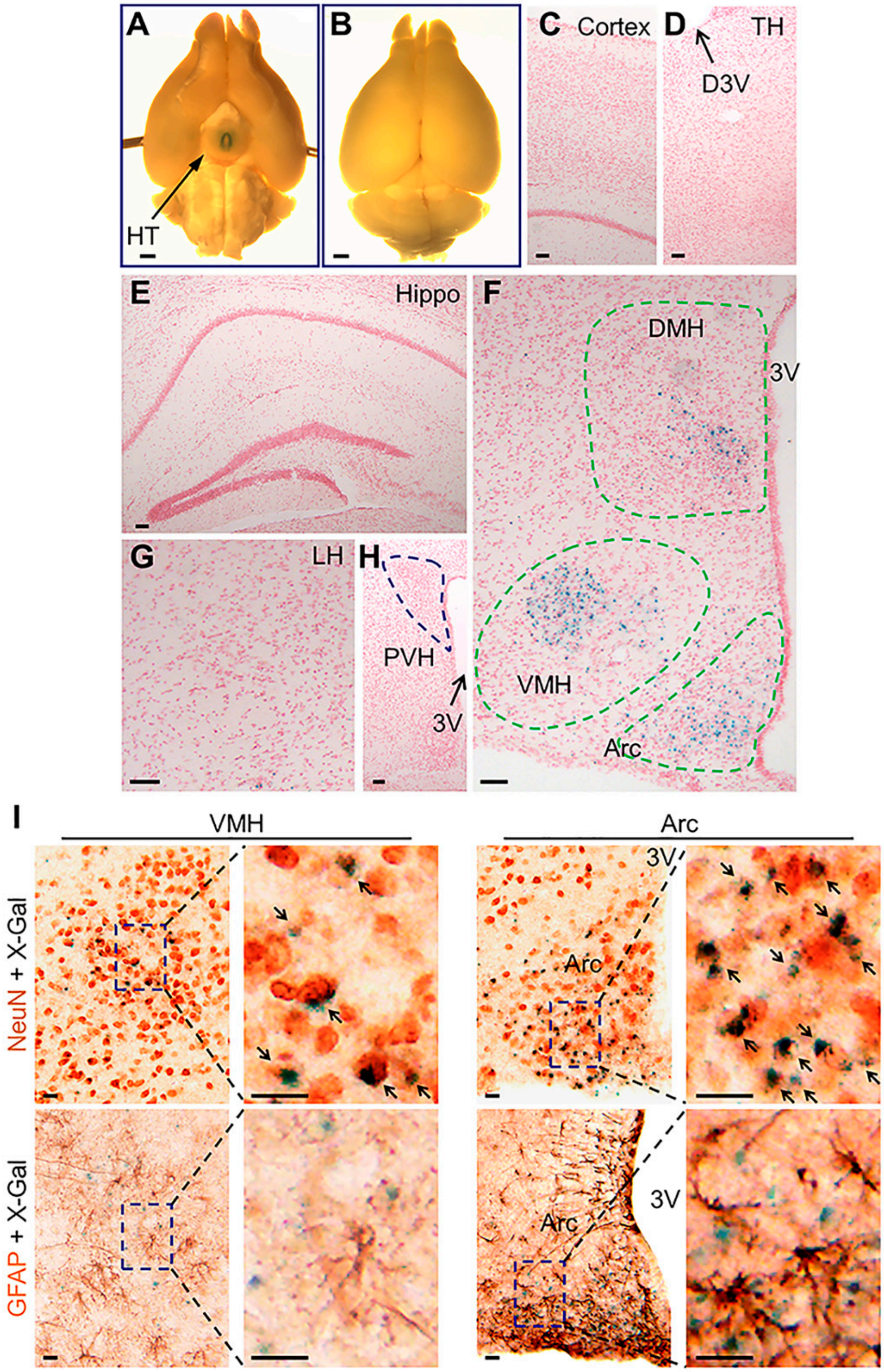

Fig. 1. Expression of E-Syt3 in mouse hypothalamus. (*A* and *B*) The whole-mount X-Gal staining of the adult *E-Syt3* heterozygous mouse brain. Ventral (*A*) and dorsal (*B*) views are shown. HT, hypothalamus. (Scale bars, 1 mm.) (*C*–*E*) Representative images showing X-Gal staining of cerebral cortex (*C*), thalamus (TH, *D*) and hippocampus (Hippo, *E*). D3V, dorsal third ventricle. (Scale bars, 50 μm.) (*F*) A representative image showing X-Gal staining product appears in the Arc, VMH, and DMH nuclei of the hypothalamus. Dashed line in green indicates the border of the nucleus. 3V, ventral third ventricle. (Scale bar, 50 μm.) (*G* and *H*) X-Gal staining of the lateral hypothalamic area (LH, *G*) and the paraventricular nucleus of hypothalamus (PVH, *H*). (Scale bars, 50 μm.) (*I*) Combined X-Gal staining for *E-Syt3* and immunohistochemical staining for NeuN and glial fibrillary acidic protein (GFAP) of the hypothalamus of *E-Syt3* heterozygous mice. X-Gal staining product appears blue, and immunohistochemical staining product appears red to brown. Arrows indicate double positive cells. (Scale bars, 20 μm.) For each staining, similar data were obtained from 4 or more mice.

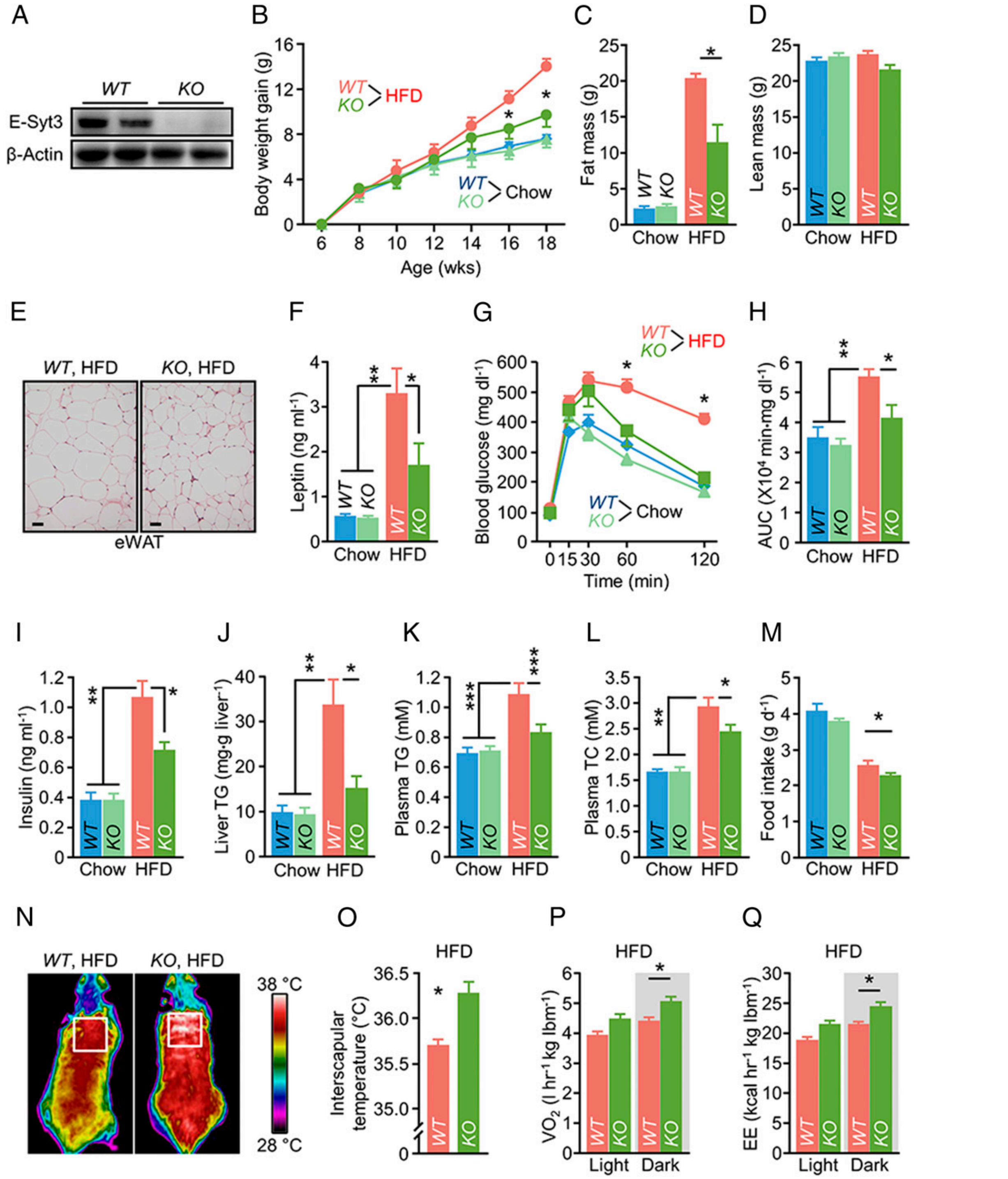

Fig. 2. Ablation of *E-Syt3* ameliorates DIO and related comorbidities. (*A*) Western blot data showing that E-Syt3 protein is depleted in the hypothalamus of *E-Syt3 KO* mice. β-Actin was used as a loading control. (*B*) Body-weight gain in male *E-Syt3 WT* and *KO* mice fed a chow or HFD from 6 wk of age. $n = 9$ (*WT*, Chow), 8 (*KO*, Chow), 6 (*WT*, HFD), 7 (*KO*, HFD). (*C* and *D*) Fat mass (*C*) and lean mass (*D*) at 36 wk old. $n = 7$ (*WT*, Chow), 8 (*KO*, Chow), or 6 (HFD) per group. (*E*) Hematoxylin & eosin (H & E) staining of the eWAT of HFD-fed mice. (Scale bars, 50 μm.) (*F*) Plasma leptin levels. $n = 8$ (Chow) or 7 (HFD) per group. (*G* and *H*) GTT (*G*) and the AUC of GTT (*H*) of 32-wk-old mice. $n = 8$ (Chow), 6 (*WT*, HFD), or 7 (*KO*, HFD) per group. (*I*) Plasma insulin levels. $n = 8$ (*WT*, Chow), 7 (*KO*, Chow), 5 (*WT*, HFD), or 6 (*KO*, HFD). (*J*) Liver TG levels. $n = 9$ (*KO*, HFD) or 10 (all other groups) per group. (*K*) Plasma TG levels. $n = 13$ (*WT*, Chow), 15 (*KO*, Chow), or 8 (HFD) per group. (*L*) Plasma TC levels. $n = 11$ (Chow) or 13 (HFD) per group. (*M*) Food intake assessed during the first 7 wk of diet treatment. $n = 10$ (*WT*, Chow), 7 (*KO*, Chow), 6 (*WT*, HFD), or 7 (*KO*, HFD). (*N* and *O*) Representative infrared images of HFD-fed *E-Syt3 WT* and *KO* mice (*N*), and the mean temperature in the interscapular (boxed) area (*O*). $n = 8$ per group. (*P* and *Q*) O_2 consumption (VO_2, *P*) and energy expenditure (EE, *Q*) of the mice fed an HFD for 6 wk. Light: light cycle; Dark: dark cycle. lbm, lean body mass. $n = 4$ per group. Data are presented as means ± SEM. $^*P < 0.05$, $^{**}P < 0.01$, $^{***}P < 0.001$, two-tailed Student's *t* test (*O*); one-way ANOVA with Newman–Keuls posthoc test (*C*, *F*, *H*–*M*, *P*, and *Q*); two-way ANOVA with Bonferroni's posthoc test, comparison between *E-Syt3 WT* and *KO* mice fed an HFD (*B* and *G*).

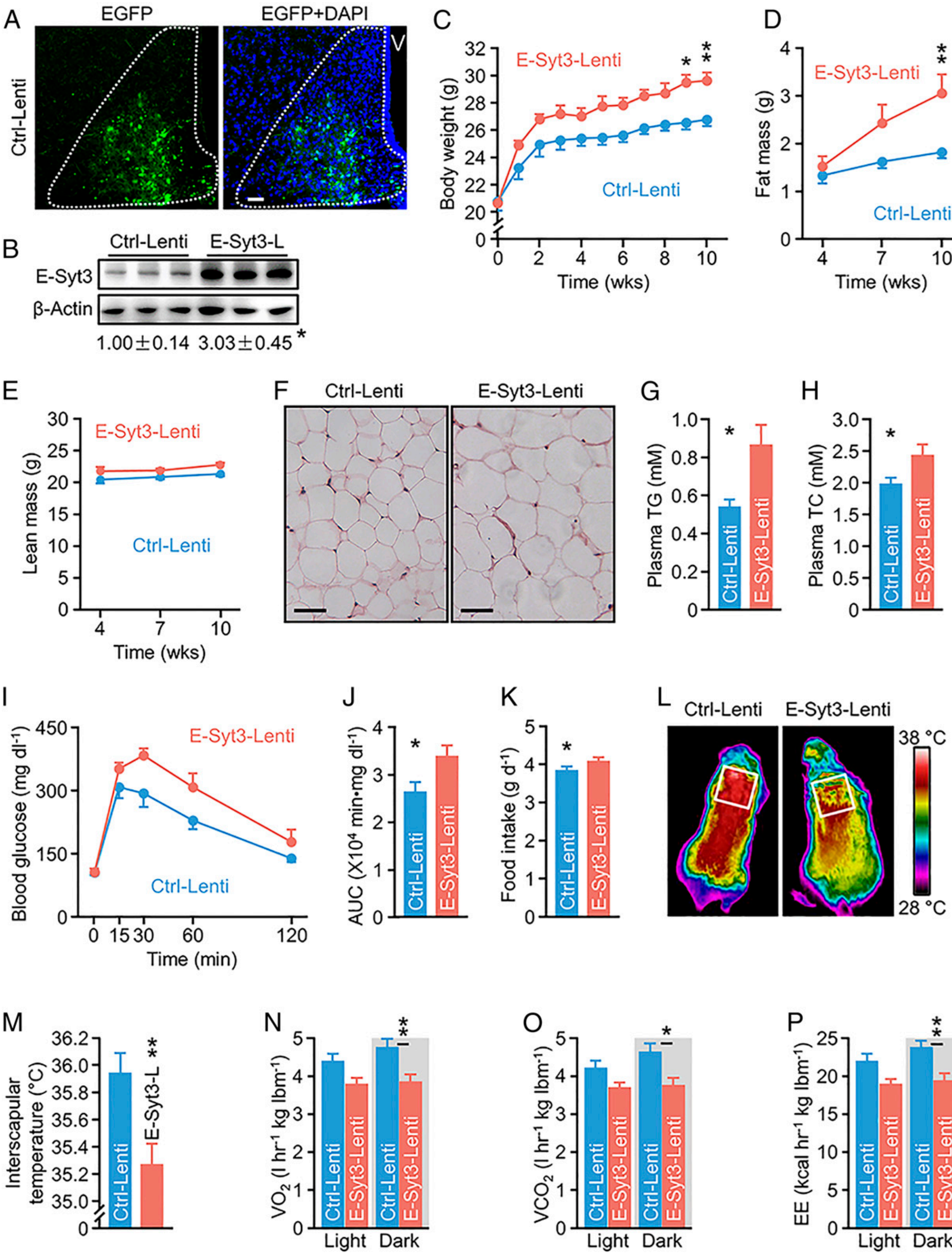

Fig. 3. Overexpression of E-Syt3 in Arc neurons leads to obesity-like phenotype. (*A*) Representative fluorescent images showing the expression of EGFP after the injection of control lentivirus (Ctrl-Lenti) into the Arc nucleus (outlined by white dotted line). Cell nuclei were counterstained with DAPI (blue). V, third ventricle. (Scale bar, 50 μm.) (*B*) Male *E-Syt3 WT* mice were injected Ctrl-Lenti or E-Syt3–Lenti viruses into Arc nucleus. Western blot for E-Syt3 in the Arc nucleus and the quantification data are shown. β-Actin was used as a loading control. $n = 3$ per group. (*C–E*) Body weight (*C*), fat mass (*D*), and lean mass (*E*) of mice after lentivirus injection. $n = 7$ per group. (*F*) Representative H&E staining images of eWAT. (Scale bars, 50 μm.) (*G* and *H*) Plasma levels of TG (*G*) and TC (*H*). $n = 7$ (*G*) or 8 (*H*) per group. (*I* and *J*) GTT (*I*) and the AUC of GTT (*J*). $n = 7$ per group. (*K*) Food intake of mice assessed during the first 6 wk after surgeries. $n = 8$ (Ctrl-Lenti) or 7 (E-Syt3–Lenti). (*L* and *M*) Representative infrared images (*L*), and the mean temperature in the interscapular (boxed) area (*M*). $n = 8$ per group. (*N–P*) O_2 consumption (VO_2, *N*), CO_2 production (VCO_2, *O*), and energy expenditure (EE, *P*) of the indicated mice. Light: light cycle; Dark: dark cycle. $n = 4$ per group. Data are presented as means ± SEM. $^{*}P < 0.05$, $^{**}P < 0.01$, two-tailed Student's *t* test (*B*, *G*, *H*, *J*, *K* and *M*); one-way ANOVA with Newman–Keuls posthoc test (*N–P*); two-way ANOVA with Bonferroni's posthoc test (*C* and *D*).

Appendix, Fig. S5 *A* and *B*), and this observation agrees with the weak expression of *E-Syt3* in the pituitary (*SI Appendix*, Fig. S1*F*). These mice were then subjected to an HFD from 6 wk of age. Under this condition, *POMC-Cre, E-Syt3*$^{Loxp/Loxp}$ mice gained significantly less body weight than the controls (Fig. 4*A*). This effect was mainly ascribed to the reduction in fat mass (Fig. 4 *B*–*F*). The less fat content in these mice was also consistent with a reduction in liver TG (*SI Appendix*, Fig. S5*C*) and reduced plasma levels in TG as well as TC (Fig. 4 *G* and *H*). Furthermore, glucose tolerance was improved in these *KO* mice (Fig. 4 *I* and *J*). This effect was mostly likely due to improved insulin sensitivity, since the pancreatic islets of *KO* mice were smaller compared with control mice under HFD condition (*SI Appendix*, Fig. S5 *D* and *E*). The food intake of *POMC-Cre, E-Syt3*$^{Loxp/Loxp}$ mice was reduced in comparison with the littermate controls (Fig. 4*K*). Moreover, deletion of *E-Syt3* in POMC neurons led to elevated interscapular temperature (Fig. 4 *L* and *M*), and increased oxygen consumption and energy expenditure (Fig. 4 *N* and *O*). Under chow feeding, deletion of *E-Syt3* in POMC neurons did not significantly impact animal's energy balance (*SI Appendix*, Fig. S5 *F*–*I*). Taken together, these data support a significant role for E-Syt3^{POMC} in the development of DIO.

POMC Neuronal E-Syt3 Affects Energy Balance via POMC Processing. POMC neurons are unique in that they express the polypeptide precursor POMC, which is processed to intermediate and mature peptides, including α-MSH. Furthermore, POMC neurons densely innervate neurons in the PVH and LH, and regulate the activities of these neurons by releasing α-MSH and other neurotransmitters (25). Considering the crucial role of α-MSH in energy balance, we examined its level by using an enzyme-linked immunosorbent assay (ELISA). The data showed that α-MSH was increased in the hypothalamus of HFD-fed *E-Syt3 KO* mice (Fig. 5*A*). In addition, hypothalamic content of POMC tended to be reduced, whereas the molar ratio of α-MSH versus POMC was elevated in these animals (Fig. 5 *B* and *C*). Notably, the mRNA levels of *POMC* in these mice remained comparable (Fig. 5*D*). Thus, the processing of POMC to α-MSH is elevated in HFD-fed *E-Syt3 KO* mice. Next, we asked whether blockade of melanocortin 3/4 receptor (MC3/4R) attenuates the effect of *E-Syt3* deficiency on energy balance. To do so, we placed cannula directed to the third ventricle of *E-Syt3 WT* and *KO* mice that had been fed an HFD. After recovery, these mice were intracerebroventricularly (i.c.v.) injected artificial cerebrospinal fluid (aCSF) or SHU9119, which is a potent antagonist for MC3/4R. During the following 12 h, *E-Syt3 KO* mice consumed less HFD than *WT* littermates when administered aCSF (Fig. 5*E*). Notably, blockade of MC3/4R elevated the food intake of *E-Syt3 WT* and *KO* mice to the comparable amounts (Fig. 5*E*). We also assessed the *POMC-Cre* and *POMC-Cre, E-Syt3*$^{Loxp/Loxp}$ mice, and obtained a similar result (Fig. 5*F*). In addition, blockade of MC3/4R abolished the effect of POMC neuron-specific deletion of *E-Syt3* on energy expenditure (Fig. 5 *G* and *H*). Hence, under HFD condition, increased production of α-MSH at least partially accounts for the rectification of energy balance in *E-Syt3*-deficient mice.

E-Syt3 Regulates the Transcription of *PC1/3* and *PC2* Genes. In rodents, processing of POMC to α-MSH is principally catalyzed by three proteolytic enzymes, i.e., prohormone convertase 1/3 (PC1/3), PC2, and carboxypeptidase E, to form $ACTH_{1–13}$, which is further amidated by the enzyme peptidyl α-amidating monooxygenase to generate desacetyl α-MSH (26). Desacetyl α-MSH is the predominant form of α-MSH in the rodent hypothalamus; however, it can be further acetylated by *N*-acetyltransferase to form α-MSH. The enhanced processing of POMC to α-MSH in *E-Syt3 KO* mice prompted us to ask whether the expression of these enzymes is changed. Our data showed that the mRNA levels of *PC1/3* and *PC2* were elevated in the hypothalamus of *E-Syt3 KO* mice (Fig. 5*I*). Western blot data further displayed that the protein levels of both enzymes were increased in chow-, 2-, and 4-wk HFD-fed *E-Syt3 KO* mice (Fig. 5 *J* and *K*). Next, we interrogated the mechanism of increased mRNA levels of *PC1/3* and *PC2* in *E-Syt3 KO* mice. In the literature, E-Syt plays a crucial role in lipid homeostasis in the cell (5). Depletion of *E-Syt* leads to elevated level of diacylglycerol (DAG) in the PM following PtdIns(4,5)P_2 hydrolysis by phospholipase C (PLC) (5). It is also known that DAG is an intracellular second messenger that allosterically activates PKC. To examine whether ablation of *E-Syt3* impacts the activity of PKC, we performed a PKC kinase activity assay, and the data showed that PKC activity was increased in HFD-fed *E-Syt3 KO* mice (Fig. 5*L*). Within the cell, activated PKC induces the expression of c-Fos (27), which then dimerizes with c-Jun to form activator protein-1 (AP-1) complex, and translocates to cell nucleus to regulate the transcription of target genes. Moreover, a prior study showed that the mRNA level of *PC1/3* was increased after the cells were treated with phorbol 12-myristate 13-acetate (28), a potent PKC activator (29). Our findings above can suggest that E-Syt3 might suppress the transcriptional activities of *PC1/3* and *PC2* genes, whereas knockdown of *E-Syt3* would do the opposite.

Subsequently, we utilized an in vitro neuronal cell line Neuro2a to address the relationship among *E-Syt3*, *PC1/3*, or *PC2* genes, and PKC-AP-1 axis. Cells were transfected with E-Syt3-Lenti or E-Syt3–Crispri-Lenti plasmids and Western blots confirmed that they successfully increased or decreased the protein levels of E-Syt3 (*SI Appendix*, Fig. S6 *A* and *B*). Our results showed that overexpression of E-Syt3 significantly decreased, whereas knockdown of *E-Syt3* by Crispri–Lenti increased the promoter activities of *PC1/3* and *PC2* genes (Fig. 5 *M*–*P*). Furthermore, when the activity of PKC or AP-1 was inhibited by Calphostin C or SR11302, the effect of knockdown of *E-Syt3* was largely abolished (Fig. 5 *O* and *P*). We also used chromatin immunoprecipitation assays to determine if AP-1 associates directly with the *PC1/3* and *PC2* promoters in Neuro2a cells. To do this, we used an antibody against c-Fos to sediment chromatins. Our data indicated that c-Fos, and presumably AP-1, is moderately enriched in the promoter regions containing the putative AP-1 binding site in both genes (*SI Appendix*, Fig. S6 *C* and *D*). Knockdown of *E-Syt3* increased the enrichments of c-Fos in the promoters of both genes (*SI Appendix*, Fig. S6 *C* and *D*). Collectively, these data indicate that *E-Syt3* has a negative role in controlling the transcriptional activities of *PC1/3* and *PC2* genes via the PKC-AP-1 axis.

Ablation of *E-Syt3* Partially Relieves ER Stress in the Hypothalamus of DIO Mice. In addition, we explored if E-Syt3 might affect hypothalamic ER stress, another important event in hypothalamic mechanism of DIO (30, 31), and indeed ER stress can impair POMC processing (20). We examined whether ablation of *E-Syt3* could impact HFD feeding-induced ER stress in the hypothalamus. Consistent with previous knowledge, our Western blot data showed that ER stress occurs in the hypothalamus of HFD-fed control mice, as indicated by the increased phosphorylation of protein kinase RNA-like endoplasmic reticulum kinase (PERK) and elevated protein levels of Xbp-1s (spliced form of X-box binding protein 1) and C/EBP homologous protein (Chop) (*SI Appendix*, Fig. S6 *E* and *F*). Of note, ablation of *E-Syt3* dramatically improved ER stress in the hypothalamus of HFD-fed mice, although it did not impact it in chow-fed controls

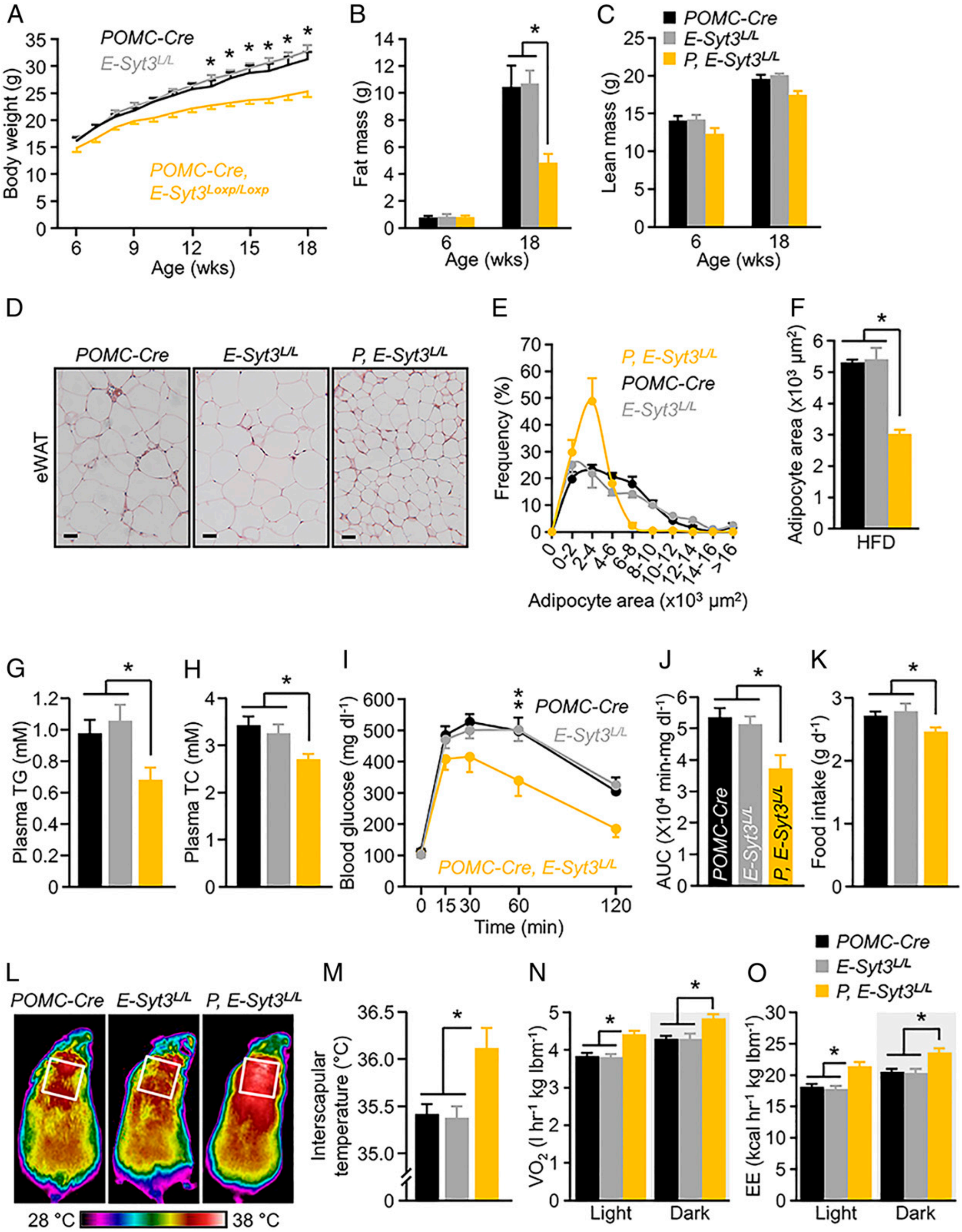

Fig. 4. POMC neuron-specific deletion of *E-Syt3* mitigates DIO and related metabolic disorders. (*A*–*C*) Male mice were placed on an HFD starting at 6 wk old. Body weight (*A*), fat mass (*B*), and lean mass (*C*) were then assessed. n = 11 (*A*), 11 (*E-Syt3*$^{Loxp/Loxp}$ in *B* or *C*) or 10 (other groups in *B* or *C*) per group. (*D*) Representative H&E staining images of eWAT. (Scale bars, 50 μm.) (*E* and *F*) Distribution of area (*E*) and the mean area of eWAT adipocyte (*F*). *E-Syt3*$^{L/L}$, *E-Syt3*$^{Loxp/Loxp}$; *P, E-Syt3*$^{L/L}$, *POMC-Cre, E-Syt3*$^{Loxp/Loxp}$. n = 3 per group. (*G* and *H*) Plasma levels of TG (*G*) and TC (*H*). n = 8 (*POMC-Cre*), 9 (*E-Syt3*$^{Loxp/Loxp}$, or *POMC-Cre, E-Syt3*$^{Loxp/Loxp}$) in *G*, or 6 (*H*) per group. (*I* and *J*) GTT (*I*) and the AUC of GTT (*J*). n = 9 per group. (*K*) Daily HFD intake. n = 13 (POMC-Cre), 8 (E-Syt3$^{Loxp/Loxp}$), or 9 (POMC-Cre, E-Syt3$^{Loxp/Loxp}$). (*L* and *M*) Representative infrared images of HFD-fed mice (*L*), and quantification of the mean temperature in the interscapular (boxed) area (*M*). n = 11 (*POMC-Cre*), 12 (*E-Syt3*$^{Loxp/Loxp}$), or 13 (*POMC-Cre, E-Syt3*$^{Loxp/Loxp}$). (*N* and *O*) O_2 consumption (VO_2, *N*) and EE (*O*) of HFD-fed mice. Light: light cycle; Dark: dark cycle. n = 4 per group. Data are presented as means ± SEM. *$P < 0.05$, **$P < 0.01$, one-way ANOVA with Bonferroni's (*B*, *F*, *J*, *K*, and *M*–*O*) or Newman–Keuls (*G* and *H*) posthoc test; two-way ANOVA with Bonferroni's posthoc test (*A* and *I*).

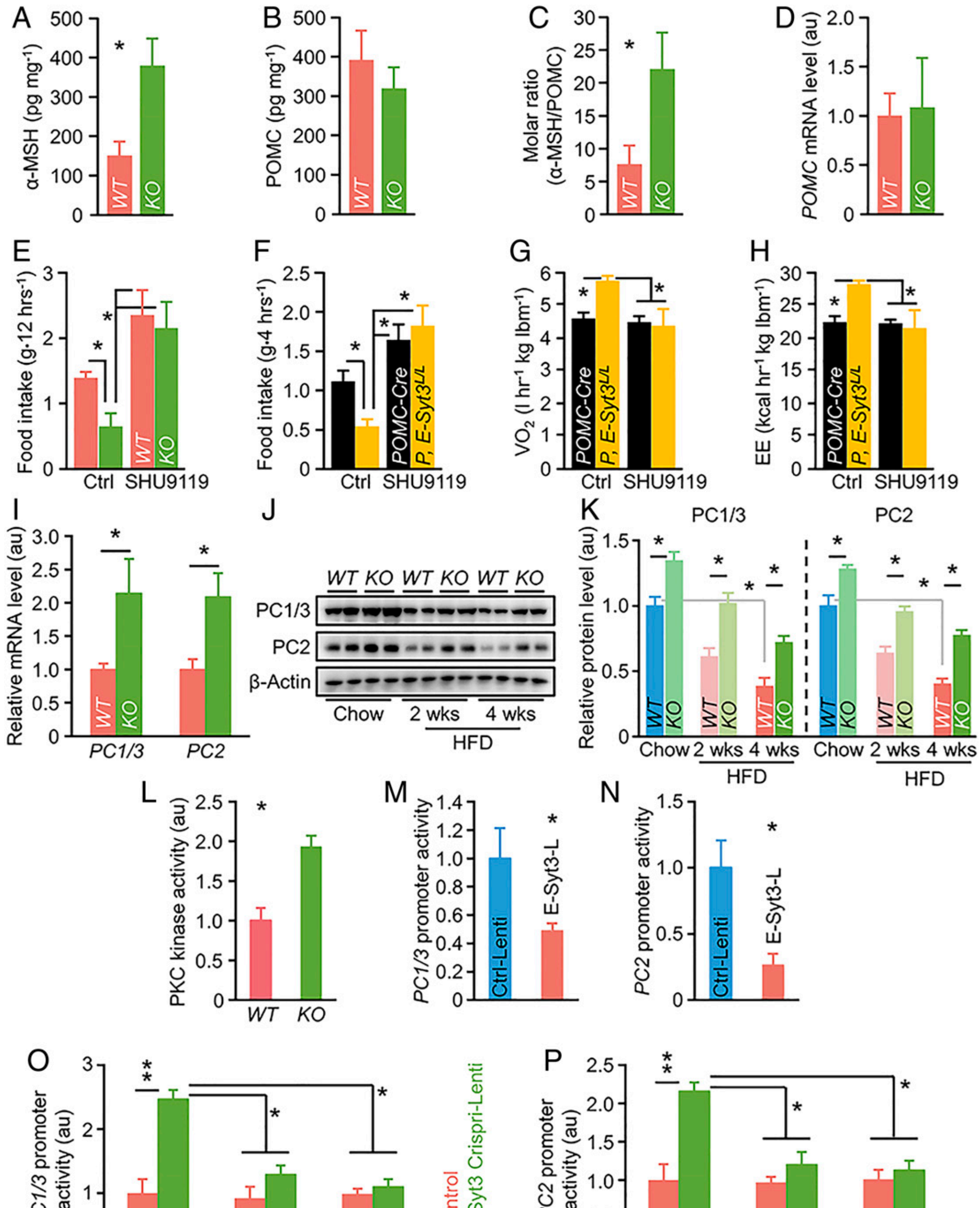

Fig. 5. Depletion of *E-Syt3* enhances the processing of POMC to α-MSH. (*A* and *B*) Hypothalamic contents of α-MSH (*A*) and POMC (*B*) peptides in HFD-fed *E-Syt3 WT* and *KO* mice. $n = 7$ (*A*) or 8 (*B*) per group. (*C*) Molar ratio of α-MSH versus POMC. $n = 7$ per group. (*D*) Relative mRNA level of *POMC* in the hypothalamus of HFD-fed mice. $n = 7$ (*WT*) or 6 (*KO*) per group. (*E*) HFD-fed mice were briefly fasted, and then i.c.v. administered SHU9119, a potent MC3/4R antagonist, or aCSF as control. Food intake during the following 12 h is shown. $n = 6$ per group. (*F*) HFD-fed mice were briefly fasted, and then i.c.v. administered aCSF or SHU9119. Food intake during the following 4 h is shown. *P, E-Syt3^{L/L}*, *POMC-Cre, E-Syt3^{Loxp/Loxp}*. $n = 6$ (Ctrl), 8 (*POMC-Cre*, SHU9119), and 7 (*POMC-Cre, E-Syt3^{Loxp/Loxp}*, SHU9119) per group. (*G* and *H*) HFD-fed mice were i.c.v. injected aCSF or SHU9119. O_2 consumption (VO_2, *G*) and EE (*H*) at 6-h posttreatment are shown. $n = 4$ per group. (*I*) Relative hypothalamic mRNA levels of *PC1/3* and *PC2* in HFD-fed mice. au, arbitrary unit. $n = 5$ (*WT*) or 7 (*KO*) in *PC1/3* assay; $n = 8$ (*WT*) or 7 (*KO*) in *PC2* assay. (*J*) Representative Western blots for PC1/3 and PC2 in the hypothalamus of chow-, 2-, and 4-wk HFD-fed mice. β-Actin was used as a loading control. (*K*) Quantification of the Western blots for PC1/3 and PC2. $n = 3$ per group. (*L*) Elevated PKC kinase activity in the Arc of HFD-fed *E-Syt3 KO* mice. $n = 7$ per group. (*M* and *N*) Overexpression of E-Syt3 (E-Syt3-L) reduced the promoter activities of mouse *PC1/3* (*M*) and *PC2* (*N*) genes in Neuro2a cells. $n = 6$ (*M*) or 3 (*N*) per group. (*O* and *P*) Crispri-mediated knockdown of *E-Syt3* increased the promoter activities of mouse *PC1/3* (*O*) and *PC2* (*P*) genes in Neuro2a cells, while suppressing the activity of PKC by Calphostin C, or the activity of AP-1 by SR11302, significantly abolished these effects (*O* and *P*). In *O* $n = 9$ (DMSO, dimethyl sulphoxide), 3 (Calphostin C), 6 (SR11302); in *P*, $n = 9$ (DMSO), 6 (Calphostin C), or 3 (SR11302) per group. Data are presented as means ± SEM. *$P < 0.05$, **$P < 0.01$, two-tailed Student's *t* test (*A*, *C*, *I*, and *L*–*N*); one-way ANOVA with Fisher's LSD (*E* and *F*), Newman–Keuls (*G* and *H*) or Bonferroni's (*K*, *O,* and *P*) posthoc test.

(*SI Appendix*, Fig. S6 *E* and *F*). Taken together, suppression of *E-Syt3* can reduce the extent of HFD feeding-induced hypothalamic ER stress.

Discussion

Here we show that E-Syt3 expressed in hypothalamic neurons plays a crucial role in DIO. Whole-body or POMC neuron-specific deletion of *E-Syt3* leads to protective effects against obesity. Of note, E-Syt3 is expressed in the VMH, DMH, and Arc nuclei. In the Arc nucleus, there are various types of neuron, including those expressing orexigenic AgRP neuropeptide. All these nuclei and cells are key nodes in the brain circuits coordinating energy balance. Elucidation of the role of E-Syt3 expressed in these nuclei and cells is important for a complete understanding of its function in energy balance and DIO. In addition, E-Syt3 can form heterodimers with E-Syt1 or E-Syt2; whether these proteins are involved in the hypothalamic regulation of energy balance needs further studies. Also, we show that the processing of POMC to α-MSH was increased in the *E-Syt3 KO* mice fed an HFD, suggesting that E-Syt3 acts as a molecular rheostat that limits the processing of POMC in DIO mice. We further show that deletion of *E-Syt3* led to the increased expression of *PC1/3* and *PC2*, which was mediated by PKC and AP-1. In *E-Syts*–deficient cells, there was sustained accumulation of DAG in the PM after the activation of PLC (5). This result agrees with our finding that the kinase activity of PKC was elevated in the hypothalamus of *E-Syt3 KO* mice, given that DAG is an allosteric activator of PKC. Previously, a study showed that leptin elevates the expression of *PC1/3* and *PC2* in hypothalamic neuronal culture and in the PVH of rats with normal body weight (32). In our study, the protein levels of PC1/3 and PC2 were reduced in HFD-fed mice. This discrepancy might be due to leptin resistance, i.e., the diminished response to leptin in DIO mice (33).

A previous study showed that blockade of PKCα and PKCβ evokes ER stress in pancreatic cells (34). This finding agrees with our results, since ablation of *E-Syt3* leads to the activation of PKC and the attenuation of ER stress in the hypothalamus of HFD-fed mice. This activation of PKC might, presumably, ameliorate ER stress in the hypothalamus. In addition, alleviation of ER stress can restore the production of α-MSH (20). Hence, both the PKC-AP-1 and the PKC-ER stress pathways might be involved in the enhanced processing of POMC in HFD-fed *E-Syt3 KO* mice. It is known that PKC plays a significant role in neuronal activation. For instance, activation of PKC increases the neuronal activities in the anterior hypothalamic area (35). Moreover, activation of PKC could increase the neuronal excitability of striatal cholinergic interneurons (36). Given that depletion of E-Syt3 elevates PKC activity, it seems plausible that the activities of neurons, such as those expressing POMC, are increased in the *KO* mice. In summary, our study shows that hypothalamic E-Syt3 plays a crucial role in DIO. Protection against obesity in *E-Syt3*–deficient mice is ascribed to the increased processing of POMC to α-MSH. These findings suggest targeting hypothalamic E-Syt3 might be a relevant strategy to counteract obesity.

Materials and Methods

Detailed information is provided in *SI Appendix*, which includes mice, plasmid construction, lentivirus production, surgery, food intake, indirect calorimetry, glucose tolerance test, lipid assay, thermography, histology, X-Gal staining, combined X-Gal and immunohistochemical staining, POMC and α-MSH assays, RT-PCR, Western blot, PKC kinase activity assay, dual luciferase reporter assay, chromatin immunoprecipitation assay, and statistics. All animal experiments were approved by the institutional animal care and use committee of the Huazhong University of Science and Technology.

MEDICAL SCIENCES

Data Availability. All data supporting the findings of this paper are available within the article and *SI Appendix*.

ACKNOWLEDGMENTS. We thank Drs. Minmin Luo and Cheng Zhan (National Institute of Biological Sciences) for sharing the *POMC-Cre* mice. This work was supported by the grants from the National Natural Science Foundation of China (81573146, 91539125), the Junior Thousand Talents Program of China and the Huazhong University of Science and Technology (to G.Z.). Juxue Li was supported by the grants from the National Natural Science Foundation of China (81570774) and the National Key Research and Development Program of China (2018YFC1003504).

1. A. Persechini, N. D. Moncrief, R. H. Kretsinger, The EF-hand family of calcium-modulated proteins. *Trends Neurosci.* **12**, 462–467 (1989).
2. S. W. Min, W. P. Chang, T. C. Südhof, E-Syts, a family of membranous Ca2+-sensor proteins with multiple C2 domains. *Proc. Natl. Acad. Sci. U.S.A.* **104**, 3823–3828 (2007).
3. F. Giordano *et al*., PI(4,5)P($_2$)-dependent and Ca(2+)-regulated ER-PM interactions mediated by the extended synaptotagmins. *Cell* **153**, 1494–1509 (2013).
4. O. Idevall-Hagren, A. Lü, B. Xie, P. De Camilli, Triggered Ca2+ influx is required for extended synaptotagmin 1-induced ER-plasma membrane tethering. *EMBO J.* **34**, 2291–2305 (2015).
5. Y. Saheki *et al*., Control of plasma membrane lipid homeostasis by the extended synaptotagmins. *Nat. Cell Biol.* **18**, 504–515 (2016).
6. C. M. Schauder *et al*., Structure of a lipid-bound extended synaptotagmin indicates a role in lipid transfer. *Nature* **510**, 552–555 (2014).
7. C. L. Chang *et al*., Feedback regulation of receptor-induced Ca2+ signaling mediated by E-Syt1 and Nir2 at endoplasmic reticulum-plasma membrane junctions. *Cell Rep.* **5**, 813–825 (2013).
8. S. Jean *et al*., Extended-synaptotagmin-2 mediates FGF receptor endocytosis and ERK activation in vivo. *Dev. Cell* **19**, 426–439 (2010).
9. A. G. Manford, C. J. Stefan, H. L. Yuan, J. A. Macgurn, S. D. Emr, ER-to-plasma membrane tethering proteins regulate cell signaling and ER morphology. *Dev. Cell* **23**, 1129–1140 (2012).
10. C. Herdman, M. G. Tremblay, P. K. Mishra, T. Moss, Loss of Extended Synaptotagmins ESyt2 and ESyt3 does not affect mouse development or viability, but in vitro cell migration and survival under stress are affected. *Cell Cycle* **13**, 2616–2625 (2014).
11. M. G. Tremblay, T. Moss, Loss of all 3 Extended Synaptotagmins does not affect normal mouse development, viability or fertility. *Cell Cycle* **15**, 2360–2366 (2016).
12. A. Sclip, T. Bacaj, L. R. Giam, T. C. Südhof, Extended synaptotagmin (ESyt) triple knock-out mice are viable and fertile without obvious endoplasmic reticulum dysfunction. *PLoS One* **11**, e0158295 (2016).
13. J. N. Campbell *et al*., A molecular census of arcuate hypothalamus and median eminence cell types. *Nat. Neurosci.* **20**, 484–496 (2017).
14. D. Huszar *et al*., Targeted disruption of the melanocortin-4 receptor results in obesity in mice. *Cell* **88**, 131–141 (1997).
15. L. Yaswen, N. Diehl, M. B. Brennan, U. Hochgeschwender, Obesity in the mouse model of pro-opiomelanocortin deficiency responds to peripheral melanocortin. *Nat. Med.* **5**, 1066–1070 (1999).
16. H. Krude *et al*., Severe early-onset obesity, adrenal insufficiency and red hair pigmentation caused by POMC mutations in humans. *Nat. Genet.* **19**, 155–157 (1998).
17. G. S. Yeo *et al*., A frameshift mutation in MC4R associated with dominantly inherited human obesity. *Nat. Genet.* **20**, 111–112 (1998).
18. C. Vaisse, K. Clement, B. Guy-Grand, P. Froguel, A frameshift mutation in human MC4R is associated with a dominant form of obesity. *Nat. Genet.* **20**, 113–114 (1998).
19. P. J. Enriori *et al*., Diet-induced obesity causes severe but reversible leptin resistance in arcuate melanocortin neurons. *Cell Metab.* **5**, 181–194 (2007).
20. I. Cakir *et al*., Obesity induces hypothalamic endoplasmic reticulum stress and impairs proopiomelanocortin (POMC) post-translational processing. *J. Biol. Chem.* **288**, 17675–17688 (2013).
21. G. Zhang *et al*., Neuropeptide exocytosis involving synaptotagmin-4 and oxytocin in hypothalamic programming of body weight and energy balance. *Neuron* **69**, 523–535 (2011).
22. L. Wu *et al*., Caffeine inhibits hypothalamic A_1R to excite oxytocin neuron and ameliorate dietary obesity in mice. *Nat. Commun.* **8**, 15904 (2017).
23. F. W. Farley, P. Soriano, L. S. Steffen, S. M. Dymecki, Widespread recombinase expression using FLPeR (flipper) mice. *Genesis* **28**, 106–110 (2000).

24. N. Balthasar *et al*., Leptin receptor signaling in POMC neurons is required for normal body weight homeostasis. *Neuron* **42**, 983–991 (2004).
25. S. T. Hentges, V. Otero-Corchon, R. L. Pennock, C. M. King, M. J. Low, Proopiomelanocortin expression in both GABA and glutamate neurons. *J. Neurosci.* **29**, 13684–13690 (2009).
26. S. L. Wardlaw, Hypothalamic proopiomelanocortin processing and the regulation of energy balance. *Eur. J. Pharmacol.* **660**, 213–219 (2011).
27. J. W. Soh, E. H. Lee, R. Prywes, I. B. Weinstein, Novel roles of specific isoforms of protein kinase C in activation of the c-fos serum response element. *Mol. Cell. Biol.* **19**, 1313–1324 (1999).
28. B. L. Mania-Farnell, I. Botros, R. Day, T. P. Davis, Differential modulation of prohormone convertase mRNA by second messenger activators in two cholecystokinin-producing cell lines. *Peptides* **17**, 47–54 (1996).
29. M. Castagna *et al*., Direct activation of calcium-activated, phospholipid-dependent protein kinase by tumor-promoting phorbol esters. *J. Biol. Chem.* **257**, 7847–7851 (1982).
30. X. Zhang *et al*., Hypothalamic IKKbeta/NF-kappaB and ER stress link overnutrition to energy imbalance and obesity. *Cell* **135**, 61–73 (2008).
31. L. Ozcan *et al*., Endoplasmic reticulum stress plays a central role in development of leptin resistance. *Cell Metab.* **9**, 35–51 (2009).
32. V. C. Sanchez *et al*., Regulation of hypothalamic prohormone convertases 1 and 2 and effects on processing of prothyrotropin-releasing hormone. *J. Clin. Invest.* **114**, 357–369 (2004).
33. W. W. Pan, M. G. Myers Jr., Leptin and the maintenance of elevated body weight. *Nat. Rev. Neurosci.* **19**, 95–105 (2018).
34. S. Ganapathy *et al*., Suppression of PKC causes oncogenic stress for triggering apoptosis in cancer cells. *Oncotarget* **8**, 30992–31002 (2017).
35. T. Kubo, Y. Hagiwara, Protein kinase C activation-induced increases of neural activity are enhanced in the hypothalamus of spontaneously hypertensive rats. *Brain Res.* **1033**, 157–163 (2005).
36. P. Deng, Z. P. Pang, Z. Lei, Z. C. Xu, Excitatory roles of protein kinase C in striatal cholinergic interneurons. *J. Neurophysiol.* **102**, 2453–2461 (2009).